APPROCHER LES DEUX INFINIS PAR LES ONDES ELECTROMAGNETIQUES

L'émission radio du fond du ciel au-dessous de 10 MHz
On Galactic background radiation at frequencies below 10 MHz

Alain Lecacheux[1], Milan Maksimovic[2]

[1]LESIA-Observatoire de Paris, alain.lecacheux@obspm.fr
[2]LESIA-Observatoire de Paris, milan.maksimovic@ obspm.fr

Mots clés: radioastronomie ; galaxie ; milieu interstellaire.
Keywords : radio astronomy ; galaxy ; interstellar medium.

Résumé/Abstract

Aux grandes longueurs d'onde, le signal radio venant du fond du ciel est la résultante des émissions et absorptions des rayonnements thermiques et non thermiques du gaz ionisé interstellaire et des radiosources discrètes galactiques et extra galactiques. Au-dessus de la fréquence de coupure ionosphérique (10-15 MHz), la distribution de brillance, maintenant bien cartographiée, est essentiellement celle d'une émission concentrée le long de l'équateur galactique, avec un maximum en direction du Centre Galactique, et d'un halo plus diffus qui décroit en intensité vers les pôles. Au-dessous de 10 MHz, faute de résolution spatiale de la part des radiomètres embarqués sur satellite, la distribution de brillance du ciel en radio reste très mal connue. Quelques rares observations depuis le sol, dans des conditions extrêmes, et les prédictions théoriques, suggèrent une situation inverse: l'équateur galactique en absorption et l'émission plutôt concentrée vers les hautes latitudes. En utilisant les données d'expériences de radioastronomie spatiale récentes (Cassini/RPWS par exemple), équipées de corrélateurs analysant plusieurs antennes filaires en rotation avec le satellite, nous montrons en effet qu'entre 10 et 1 MHz la distribution de brillance évolue graduellement d'une situation à l'autre. Nous décrivons la méthode, ses limitations, et les implications astrophysiques du résultat.

The brightness distribution of the radio sky is nowadays well documented in the part of the radio spectrum above Earth's ionosphere cut-off. As the result of emissions and absorptions of thermal and non-thermal radiations from interstellar ionized gas and discrete radio sources, the brightness is concentrated along the Galactic Equator, mainly towards the Galactic Centre. In the frequency range not available from the ground and lacking of instrumentation with spatial resolution capability (typically below 10 MHz), theoretical predictions and a few observations indicated that the maximum sky brightness would be rather located at much higher galactic latitudes. By analysing data from a radio spectrometer using a spinning, tri-axial antenna system (e.g. Cassini/RPWS), we confirm that the overall galactic brightness distribution gradually evolves from equatorial to polar, when frequency is decreasing. We describe our method of analysis, its limitations and discuss astrophysical implications of the result.

1 Introduction

Among the wealth of contributions to the knowledge of the Universe brought to us by the Radio Astronomy, a basic one is the appearance of the whole (radio) sky as a function of the frequency. Its description has well progressed in the two last decades thanks to the development of powerful radio imaging techniques and also because of the necessity to clean the newly obtained Cosmic Microwave Background maps from all foreground contaminations.

In the frequency range available from the ground (say from about 30 MHz to 100 GHz and above), the overall picture is now well described and understood [1]: it is dominated by an anisotropic diffuse component, concentrated along the Galactic Equator (the plane of our Galaxy), mainly in direction of the Galactic Centre (Sgr A), The observed brightness is a combination of thermal emission and absorption by the galactic warm ionized gas (mainly HII) and of non-thermal emission by the galactic relativistic electrons. A second weaker component, likely to be isotropic, is due to the large (infinite ?) amount of emitting extragalactic radio sources lying in every direction. Since the free-free optical depth of such a medium varies with the frequency (as $\nu^{-2.1}$), the relative contrast of the various visible structures is changing with the frequency, but the large scale features remain similar over the whole spectrum [1]. An example of such a sky radio map, which was recently obtained at the frequency of 45 MHz [2], is shown in Fig. 2a.

In the frequency range blocked by Earth's ionosphere (from about 30 MHz or below), the appearance of the radio sky is much less documented. In space, techniques are not yet available to directly make maps with angular resolution comparable to what can be done from the ground. However, a few observations from the ground, made in special conditions, indicate that the sky appearance, regarding its brightness distribution, might be very

different in the lowest frequency range. For instance, taking good advantage of an ionospheric hole over Tasmania, Reber [3], then Ellis [4] were able to observe sky at frequencies as low as 2 MHz, measuring a much higher brightness at the South Galactic Pole than at the Equator.

Even more convincing, - and this time by using a space borne experiment -, Manning and Dulk [5] were using radio data from the WIND spinning spacecraft and suggested that the sky brightness maximum location moves from the Galactic Centre to the Poles when the observing frequency varies from 10 down to 1 MHz. They were using the modulated antenna response due to the spacecraft spin, but in a somewhat qualitative way. As stated in their paper: "as the antenna rotates, the received intensity varies from a maximum approximately when the antenna is broadside to the regions of lowest brightness". The aim of the present paper is to investigate what can be ultimately done with such a space experiment, - say, a wideband spectrometer fed to a system of wire antennas aboard a spinning spacecraft -. In section 2, we present a quantitative formulation of the problem. In section 3 we show an example of application obtained by using the Cassini/RPWS instrument en route to Saturn. The results are briefly discussed in section 4.

2 What can be actually obtained by using a radiometer on a single spacecraft ?

In the fields of solar and planetary space radio astronomy, there is an abundant literature on spinning radio antennas (for instance [6], [7], [8]). The method was mostly used for studying small size radio sources, so that only the simplest point source case was deeply analysed. Applying those simple analyses to the extended case of the galactic radiation is clearly not satisfying. However, it is known for a long time ([3], [4]) that the galactic background can modulate the antenna output at a significant level, only depending on the sensitivity of the receiving system.

Our method of analysis starts with the basic relationship between the incident electric field and the antenna output voltage, here written in the (frequency) Fourier domain as a scalar product of complex quantities:

$$V(\omega) = H^{\dagger} E(\omega) \tag{1}$$

The factor H is the impulse response of the antenna, considered as a linear (filtering) device. It is otherwise known as the antenna *effective length* vector. The latter can also be modelled as the Fourier transform of the (steady) current established on the antenna body. In the case of a system of several antennas, the equation (1) still hold: H becomes a matrix and V is the vector of the corresponding antenna output voltages. Effective lengths are most often considered in projection onto the plane perpendicular to the wave vector (which contains the incident electric field for a source at infinite distance). Here we will rather characterize the antenna(s) by their effective lengths expressed in some working reference frame (for instance the spacecraft XYZ reference frame) and consider the matrix R of the transformation from this frame to the wave reference frame. The basic equation read now as:

$$V = (RH)^{\dagger} E$$

The covariance matrix of the measured voltages, - the final output of the system -, follows as:

$$\Gamma_A = \langle V V^{\dagger} \rangle = H^{\dagger} \, (R^T \Gamma R) \, H \tag{2}$$

where $\Gamma = \langle E E^{\dagger} \rangle$ is the coherence matrix of the incident electric field. Brackets mean integration over time. In the following, since observing frequencies are lower than 10 MHz and antenna lengths shorter than a few meters, the antennas can be considered as short with respect to the wavelength: H does not depend on the wave direction (but can depend on the frequency) and is a real vector, at least within a reasonable approximation. The matrix $C_0 = R^T \Gamma R$ contains most of the information available from the observed electromagnetic wave (namely its direction, intensity and polarisation).

Let consider the brightness $B_\nu(\theta, \varphi)$ of the whole radio sky as made of individual, uncorrelated, unpolarised point sources located in each direction (θ, φ). The overall radiation from the whole sky is then characterized by:

$$C_{4\pi} = \iint C_0(\theta, \varphi) \sin\theta \, d\theta \, d\varphi = \iint B_\nu(\theta, \varphi) \, M(\theta, \varphi) \sin\theta \, d\theta \, d\varphi$$

in which $M(\theta, \varphi)$ is some matrix (not shown here for saving space) containing sine and cosine combinations up to the power of 2.

Now the $B_\nu(\theta, \varphi)$ function, defined on the 2-sphere S_2, can be developed in a series of orthogonal spherical harmonics Y_l^m, as:

$$B_\nu(\theta,\varphi) = \sum_l \sum_{|m|\le l} b_{l,m} Y_l^m(\theta,\varphi) \tag{3}$$

together with the reciprocal formula: $b_{l,m} = \iint B_\nu(\theta,\varphi)\, \bar{Y}_l^m(\theta,\varphi) \sin\theta\, d\theta\, d\varphi$. The $b_{l,m}$ are complex numbers, often described as the Fourier coefficients of the expansion (3) on the sphere S_2. Substituting in the above integral, one obtains:

$$C_{4\pi} = \sum_l \sum_{|m|\le l} b_{l,m} \iint Y_l^m(\theta,\varphi)\, M(\theta,\varphi) \sin\theta\, d\theta\, d\varphi$$

One can easily check that all the integrals in previous formula vanish, except those for $l = 0$ and $l = 2$, so that one get:

$$C_{4\pi} = \sqrt{\frac{2\pi}{15}} \begin{bmatrix} \frac{2\sqrt{5}\, b_{0,0} + b_{2,0}}{\sqrt{6}} - \mathrm{Re}(b_{2,2}) & \mathrm{Im}(b_{2,2}) & \mathrm{Re}(b_{2,1}) \\ \mathrm{Im}(b_{2,2}) & \frac{2\sqrt{5}\, b_{0,0} + b_{2,0}}{\sqrt{6}} + \mathrm{Re}(b_{2,2}) & -\mathrm{Im}(b_{2,1}) \\ \mathrm{Re}(b_{2,1}) & -\mathrm{Im}(b_{2,1}) & 2\frac{\sqrt{5}\, b_{0,0} - b_{2,0}}{\sqrt{6}} \end{bmatrix} \tag{4}$$

Given a particular antenna system described by the H matrix, the output of the correlator (formula (2)), corresponding to the "all sky" emission, finally read as:

$$\Gamma_A = H^\dagger\, C_{4\pi}\, H \tag{5}$$

While the actual sky map would in principle be defined by a large number of $b_{l,m}$ coefficients, the observed radio map appears to be strongly filtered into only six independent measurable quantities, namely: the real parts of $b_{0,0}$ and $b_{2,0}$, and the real and imaginary parts of $b_{2,1}$ and $b_{2,2}$ (taking into account that $b_{2,-1} = -\bar{b}_{2,1}$ and $b_{2,-2} = \bar{b}_{2,2}$ since B_ν is a real function).

A consistency check can be done by substituting in (4) the coefficients for the point source in direction (θ_0, φ_0)

$$b_{l,m}^{(0)} = \iint \delta(\theta - \theta_0, \varphi - \varphi_0)\, \bar{Y}_l^m(\theta,\varphi) \sin\theta\, d\theta\, d\varphi$$

and verifying that (4) reduces to $C_0(\theta_0, \varphi_0)$.

When the spacecraft spins and the antenna boom rotates, the signal (formula 5) is modulated at both the fundamental and first harmonics of the spin frequency [6]. The resulting Fourier series is made of three complex components, corresponding to five independent real quantities, which can be easily fitted to the data. One can show that there is a one-to-one correspondence between those spin modulation Fourier components and the $\{b_{0,0}, b_{2,m}\}$ components described above.

A single antenna on a spinning spacecraft is not enough for retrieving all the six quantities ($b_{0,0}$ and $b_{2,0}$ cannot be resolved). At least two antennas are needed, with different tilt angles with respect to the spin axis. The "ideal" configuration [11] would involve three no coplanar antennas in full correlation: all the six involved quantities can then be determined with some redundancy, what can be useful for a maximum accuracy.

Changing the working reference frame, i.e. the orientation of the spacecraft spin axis, if any, does not bring any new information. Indeed, it is well known [12] that, under a rotation, each spherical harmonic Y_l^m of degree l is transformed into a linear combination of the Y_l^m with same l degree, namely:

$$R\left(Y_l^{m'}\right)(\theta,\varphi) = \sum_{|m|\le l} Y_l^m(\theta,\varphi)\, \mathcal{D}_{m,m'}^{(l)}(R)$$

leading to the component transformation:

$$R\left(b_{l,m'}\right) = \sum_{|m|\leq l} \overline{\mathcal{D}}^{(l)}_{m,m'}(R)\, b_{l,m} \tag{6}$$

whose calculation involves the so-called Wigner-D matrices, well studied and used in quantum mechanics and particle physics [10]. From the latter result, a powerful method for precise, in flight calibration of any space borne low frequency radio astronomy instrument could be derived, based on the determination of the amplitudes and phases of the $b_{2,m}$ coefficients at each frequency.

3 An application by using data from the Cassini/RPWS instrument :

The Radio and Plasma Wave Science investigation on board of the *Cassini* Saturn's orbiter is fully described in [11]. The HFR part of the instrument mainly dedicated to radio astronomy, was designed and developed in the Space Department of the Paris Observatory in the 1990s. It is based on digital, real time, spectral correlation of several pass band filters, analyzing a set of three 10 meter long, wire antennas. The analyzed frequency range extends from about 1 kHz to 16 MHz.

While *Cassini* orbiter was originally designed as a 3-D stabilized spacecraft, rolling the whole spacecraft about various axes was a thoroughly used method to move on board scientific instruments on their target, as well as for calibrating and doing general housekeeping. Many thousands of such roll manoeuvres are available throughout the life of *Cassini*.

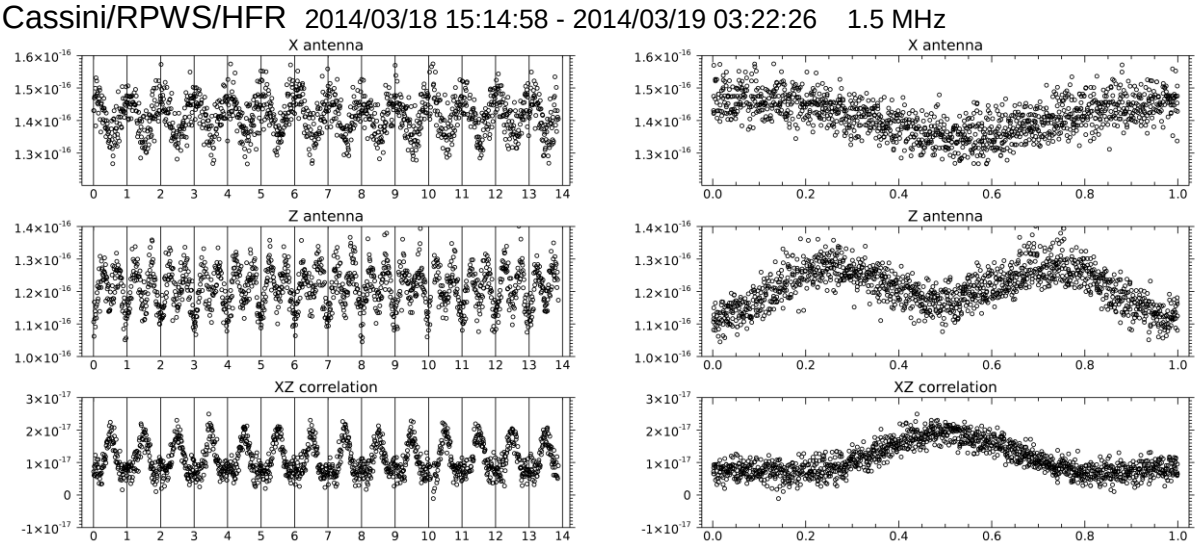

Figure 1 : Example of a Cassini roll maneuver, lasting about 12 hours on 2014, March 18. The left panel shows full time waveforms of the available output at 1.6 MHz from one pair of RPWS monopole antennas (X and Z). The horizontal axis is graduated in number of rotations at the rate of 2 milliRad/sec. The vertical axis is expressed in V^2Hz^{-1} at the receiver input. In the right panel, the same data are displayed, but after folding the rotation phase. The modulation amplitude, of the order of 20% of the DC level, is well measurable in spite of the instrumental noise due to the spectral analysis.

Fig.1 shows an example of a long lasting roll manoeuvre, dedicated to in flight calibration of another on board scientific instrument. The right panel displays the waveforms, at the frequency of 1.5 MHz, of the $\langle XX^* \rangle, \langle ZZ^* \rangle, \mathrm{Re}\langle XZ^* \rangle$ correlator output, computed by the digital receiver in real-time. Another pair of antennas (YZ) was analyzed in the same time, allowing for an accurate measurement of the coefficients of the $C_{4\pi}$ matrix given by formula (4)).

Fig.2 summarizes our final result. All six displayed maps are radio maps of the whole sky (shown in Mollweide projection, as described in the legend of the figure). The four first maps ((a) to (d)) are drawn from a reference map taken at the 45 MHz radio frequency and extracted from the low frequency sky survey by the LWA1 radio telescope [2]: the map is drawn in galactic coordinates, with an angular resolution of 3.6°. Map (b) is drawn from

the same data as map (a), but in coordinates of the spacecraft reference frame corresponding to the orientation of *Cassini* at the starting time of the manoeuvre displayed in Fig.1 and computed from the archived *Cassini* spacecraft attitude data. Map (c), still in this reference frame, was built by using formula (3) and spherical harmonics components obtained from map (b). Then, formula (6) was used to back transform map (c) into galactic reference frame, as in map (a).

Comparison of map (c) with map (b), or map (d) with map (a), illustrates the huge angular resolution loss of the method, as discussed in previous section. The comparison of map (d) with map (a) shows also that the large scale brightness distribution is not too much distorted: the maximum brightness is well found at the centre of the map, the poles have much lower intensities, as expected. Replication at 180° of the bright central patch is an artefact due to the absence of $b_{1,m}$ harmonics (or, equivalently, due to the dipolar antenna beam symmetry between any direction and its anti-direction).

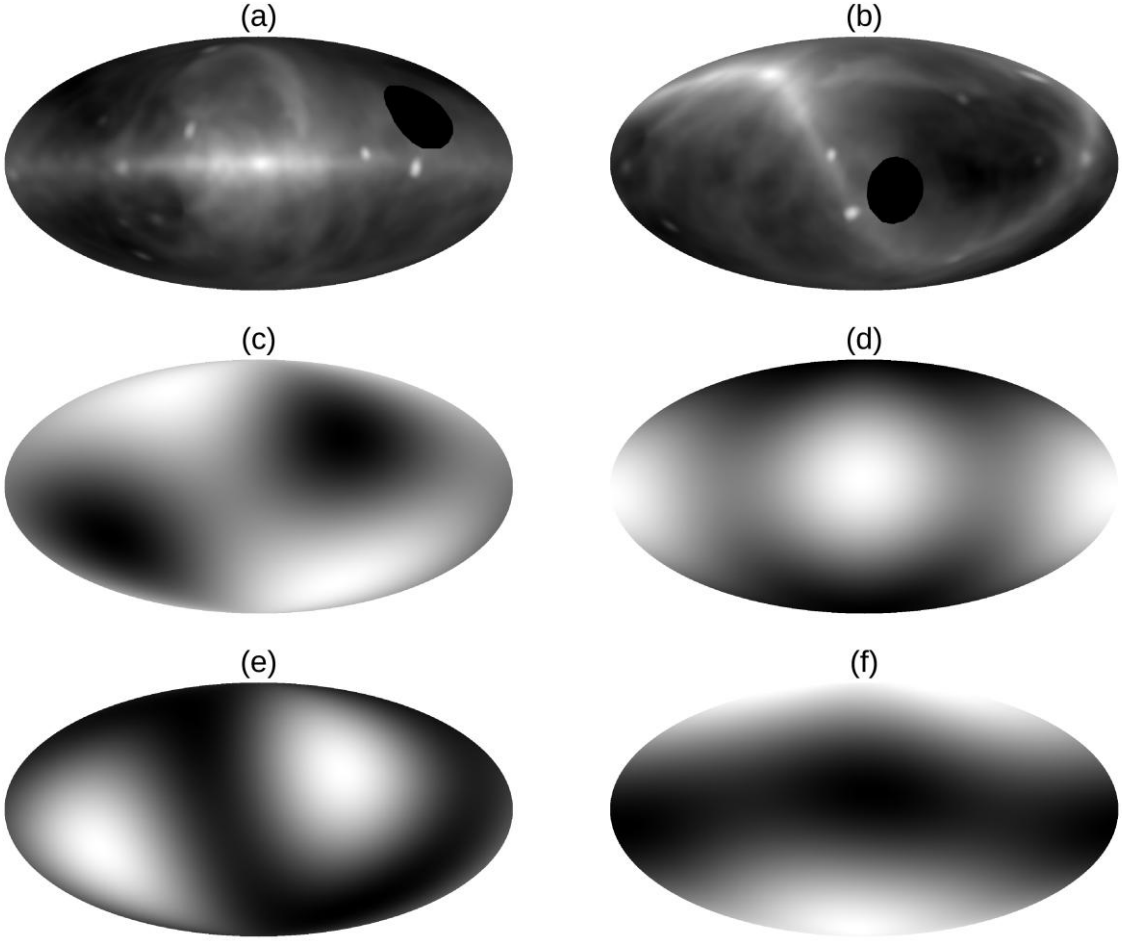

Figure 2 : six radio maps of the whole sky, drawn in Mollweide projection (North pole at the top; increasing longitudes from left (-180°) to right(+180°)). (a) reference map (45 MHz) in galactic coordinates; (b) same map but; (c) same as (b), but after antenna "filtering"; (d) back to galactic reference frame, to be compared to (a); (e) real measurement in the S/C reference frame, done at 1.5 MHz, by using Cassini/RPWS/HFR data; (f) back to galactic reference frame, to be compared to (a). See text for details.

The two last maps ((e) and (f)) are built by using the data (Fig.1) actually measured at much lower radio frequency, namely 1.5 MHz. Map (e) results from applying formula (3) as in case of map (c). Map (f) is the transformation into galactic coordinates by applying formula (6).

Clearly, passing from map (a) (or (d)) to map (f), that is from frequency range lying above to below 10 MHz, exchanges bright and dark regions. At 1.5 MHz, the galactic poles unambiguously appear to be much more brighter than the equator with, maybe, an excess of brightness at the South pole over the North one.

4 Discussion

Our result is not completely surprising: it is the confirmation of previous observations, as stated in the introduction. But for the first time, at our knowledge, one can get a clear evidence that the radio sky appearance is drastically changing when the observing frequency is decreasing from above to below 10 MHz.

The main reason is the presence within the galactic interstellar medium of a large amount of warm ionized gas (the so called Warm Ionized Medium), which has been inferred from other observations also. It is now believed that the WIM is responsible for producing, for instance, the diffuse optical H_α emission, the dispersion of pulsar radio signals, and the Faraday rotation observed in every direction in our Galaxy [15]. From all these observations, a general, quantitative picture of the WIM was deduced: with an average electron density of 0.025 cm^{-1} and an average temperature of 10^4 K, this is a quite irregular medium made of blobs (filling factor of ~0.1) of density 0.1-0.5 cm^{-1} and scale height of 1 kpc. Taking into account those physical properties, one can expect that the WIM optical depth is close to zero in all directions at 100 MHz and above, progressively increases with decreasing frequency in dense regions, then that the medium becomes optically thick to any radio emissions at some very low frequency (estimated to be around 4 MHz by using above numbers). For a far observer located in the periphery of the Galaxy (the case of the Solar System), the consequence is a strong extinction, from this frequency downward, of the synchrotron emission produced by the far galactic relativistic electrons, leaving only place to the emission from the local ones, within a radius of a few kpc. This absorption being likely more pronounced towards the equator than towards the poles.

If this scenario is correct, an increase of the angular resolution would show the irregularities that exist in the interstellar medium, e.g. the distribution of HII regions and dense clouds. A little bit more remains to be extracted from the existing single spacecraft radio observations. This is under study, now.

In the future, hopefully not too far, the final answer will become available when antenna arrays will be deployed on spacecraft clusters and will provide, by using interferometric technique, true detailed images of the sky background.

5 References

[1] A. de Oliveira-Costa, M. Tegmark, B. Gaensler, J. Jonas, T. Landecker et P. Reich, *MNRAS,* vol. 388, pp. 247-260, 2008.

[2] J. Dowell, G. Taylor, F. Schinzel, N. Kassim et K. Stovall, *MNRAS,* vol. 469, n° %14, pp. 4537-4550, 2017.

[3] G. Reber, *J.Franklin.Inst.,* vol. 285, pp. 1-12, 1968.

[4] G. Ellis, *Aust. J. Phys.,* vol. 35, p. 91ff, 1982.

[5] R. Manning et G. Dulk, *Astron.Astrophys.,* vol. 372, pp. 663-666, 2001.

[6] R. Manning et J. Fainberg, *Sp. Sci. Instr.,* vol. 5, p. 161ff, 1980.

[7] A. Lecacheux, *Astron. Astroph.,* vol. 70, pp. 701-706, 1978.

[8] B. Cecconi et P. Zarka, *Radio Science,* vol. 40, p. 3ff, 2005.

[9] L. Brown, *Ap.J.,* vol. 180, p. 359, 1973.

[10] J. Alexander, L. Brown, T. Clark, R. Stone et R. Weber, *Ap.J.,* vol. 157, n° %1L163, 1975.

[11] A. Lecacheux, C. Harvey et A. Boischot, *Ann. Telecomm.,* vol. 34, pp. 253-265, 1979.

[12] J. Driscoll et D. Healy, *Adv. Applied Math.,* vol. 15, pp. 202-250, 1994.

[13] M. Blanco, M. Florrez et M. Bermejo, *J. Molecular Structure,* vol. 419, pp. 19-27, 1997.

[14] D. Gurnett et e. al., «The Cassini Radio and Plasma Wave,» *Sp. Sci. rev.,* vol. 114, pp. 395-463, 2004.

[15] K. Dwarakanath, AGU Geophysical Monograph 119, R.G. Stone, K.W. Weiler, M.L. Goldstein and J.L Bougeret , 2000.